Increasing Fisher Information using Moving-Mesh Reconstruction

Qiaoyin Pan,[1,2,*] Ue-Li Pen,[2,3,4,5,†] Derek Inman,[2,6] and Hao-Ran Yu[2,7]

[1]*School of Physics, Nankai University, 94 Weijin Rd, Nankai, Tianjin, 300071, China*
[2]*Canadian Institute for Theoretical Astrophysics, University of Toronto, 60 St. George Street, Toronto, Ontario M5S 3H8, Canada*
[3]*Dunlap Institute for Astronomy and Astrophysics, University of Toronto, Toronto, ON M5S 3H4, Canada*
[4]*Canadian Institute for Advanced Research, Program in Cosmology and Gravitation*
[5]*Perimeter Institute for Theoretical Physics, Waterloo, ON, N2L 2Y5, Canada*
[6]*Department of Physics, University of Toronto, 60 St. George, Toronto, ON M5S 1A7, Canada*
[7]*Kavli Institute for Astronomy and Astrophysics, Peking University, Beijing 100871, China*

(Dated: December 9, 2016)

Reconstruction techniques are commonly used in cosmology to reduce complicated nonlinear behaviour to a more tractable linearized system. We study the Moving-Mesh algorithm which is able to consistently compute the displacement field from non-linear density fields. To quantify the algorithm's ability to reconstruct linear modes, we study the Fisher information presented in 130 N-body simulations before and after reconstruction. We find that the linear scale is pushed to $k \simeq 0.3$ h/Mpc after reconstruction. We furthermore find that the non-linear plateau of the cumulative Fisher information is increased by a factor of ~ 50 after reconstruction, from $I \simeq 2.5 \times 10^{-5}/(\mathrm{Mpc/h})^3$ to $I \simeq 1.3 \times 10^{-3}/(\mathrm{Mpc/h})^3$ at $k \simeq 2.6$ h/Mpc. This result includes the decorrelation between initial and final fields, which has been neglected in some previous studies artificially improving their performance. We expect this technique to be beneficial to problems such as baryonic acoustic oscillations and cosmic neutrinos that rely on an accurate disentangling of nonlinear evolution from underlying linear effects.

PACS numbers:

I. INTRODUCTION

Two-point statistics provide a complete description of Gaussian density fields and can be computed efficiently even for large data sets. However, non-linear gravitational evolution leads to highly non-Gaussian matter distributions which require higher order statistics to fully characterize. Such statistics are computationally expensive and can be challenging to relate to cosmological parameters. To mitigate these difficulties, it is common to transform the matter field in a way that hopefully reduces non-Gaussianity. For example, Gaussianization transforms have been used to make the logarithmic distribution more Gaussian [1, 2] and Wavelet Non-Linear Wiener filters have been used to separate Gaussian and non-Gaussian components of the density field [3–5].

The success of techniques can be quantified by computing the Fisher information presented in the power spectrum before and after reconstruction. Rimes and Hamilton [6] were the first to study the Fisher information in the non-linear matter power spectrum calculated from N-body simulations. They found that the information has a plateau on translinear scales ($k \simeq 0.2 - 0.8\ h$/Mpc) due to strong coupling of Fourier modes. Qualitatively, this means that the power spectrum on these scales gives little additional information. However, Harnois-Déraps et al. [5] computed the Fisher information for various Gaussianization methods (and combinations of methods) and found that while mode coupling is reduced, there is not necessarily an improvement in the cross correlation between the initial Gaussian density field and the final non-linear one.

In studies of Baryon Acoustic Oscillations (BAO), density fields are subjected to *reconstruction* which partially inverts non-linear evolution by applying a negative Zel'Dovich displacement field [7]. The linear density field is typically estimated via Lagrangian perturbation theory (LPT) using the linear Zel'Dovich displacement $-\nabla_q \cdot \boldsymbol{\Psi}(\boldsymbol{q})$ with respect to initial coordiantes $\boldsymbol{q}$ [8]. Recently, Zhu et al. [9] described how to use the Moving-Mesh algorithm (MM), first described in [10, 11], to efficiently estimate $\boldsymbol{\Psi}(\boldsymbol{q})$ from non-linear density fields. They further showed that even though shell-crossing and vorticity are not recovered, linear density modes are still recovered up to scales relevent to the BAO.

In this paper, we compute the Fisher information recovered after using this reconstruction scheme on 130 independent N-body simulations. The paper is organized as follows. In §II, we briefly describe the computation of the displacement potential using MM algorithm. In §III, we describe the simulations, implementation of the reconstruction and compare the power spectra and cross correlations before and after reconstruction. In §IV, we futher compute the correlation matrix and Fisher information before and after reconstruction. Finally, in §V, we summarize our results and discuss the effectiveness of the reconstruction and its potential uses.

*Electronic address: panda@mail.nankai.edu.cn
†Electronic address: pen@cita.utoronto.ca

II. RECONSTRUCTION ALGORITHM

In this section, we briefly review the MM algorithm; for a more complete description we refer the reader to [12]. The aim of the MM algorithm is to estimate the displacement of particles in Lagrangian coordiantes from their final Eulerian position only. The general principle is to relate a particle's Eulerian coordinates, x^i to a curvilinear system, ξ^μ, in which the number of particles per grid cell is approximately constant. These coordinates are related via the so-called deformation, which we assume to be a pure gradient:

$$x^i = \xi^\mu \delta^i_\mu + \frac{\partial \phi}{\partial \xi^\mu} \delta^{i\mu} \tag{1}$$

and ϕ is called the deformation potential. Numerially, we can solve iteratively for the deformation potential via the diffusion equation,

$$\partial_\mu (\rho \sqrt{g} e^\mu_i \delta^{i\nu} \partial_\nu \dot{\phi}) = \Delta\rho, \tag{2}$$

where $e^i_\mu = \partial x^i / \partial \xi^\mu$ is the coordinate transformation matrix, $\sqrt{g} \equiv \det \left| e^i_\mu \right|$ is the volume element and $\Delta\rho = \bar{\rho} - \rho\sqrt{g}$. Detailed discription of the analytical formulation were presented in [10, 11]. Eq. 2 can be solved through the use of the multigrid algorithm described in [10–12]. The displacement field is then given by

$$\boldsymbol{\Psi}(\boldsymbol{\xi}) = \nabla\phi(\boldsymbol{\xi}), \tag{3}$$

and the reconstructed density field is given by

$$\delta_R(\boldsymbol{\xi}) = -\nabla \cdot \boldsymbol{\Psi}(\boldsymbol{\xi}) = \nabla^2 \phi(\boldsymbol{\xi}). \tag{4}$$

III. IMPLEMENTATION AND POWER SPECTRA

We use the CUBEP^{3}M code [13] to run 140 simulations with a box size of 600 Mpc/h and 512^3 particles. The initial conditions are computed using the transfer function given by CAMB [14] and then propagating the power back to $z = 100$ with a linear growth factor. The Zel'dovich approximation is used to calculate the displacement and velocity fields of the particles. For these simulations, we use cosmological parameters $\Omega_M = 0.321$, $\Omega_\Lambda = 1.0 - \Omega_m$, $h = 0.67$, $\sigma_8 = 0.83$, and $n_s = 0.96$. Different random seeds are used to produce the initial conditions for different simulations so that they are independent of each other.

We use Voronoi tessellation method to estimate the density contrast $\delta_S = \delta\rho/\rho - 1$ from the particles, and then apply the MM reconstruction to these fields with a resolution of 512^3 cells. The reconstruction code solves the dispacement potentials iteratively until the root mean square (rms) of the results drop (from ~ 7.5) to 0.20. For different simulation samples, different time steps are taken to get the results of the same rms. We finally pick 130 simulation samples to do the remaining calculation, each among which gives a final rms of 0.20 through running the reconstruction code for no more than 2000 time steps. A 2-D projection of one layer of the deformed grids and the original density field on the grids are given in Fig. 1. As expected, there is no grid crossing after reconstruction.

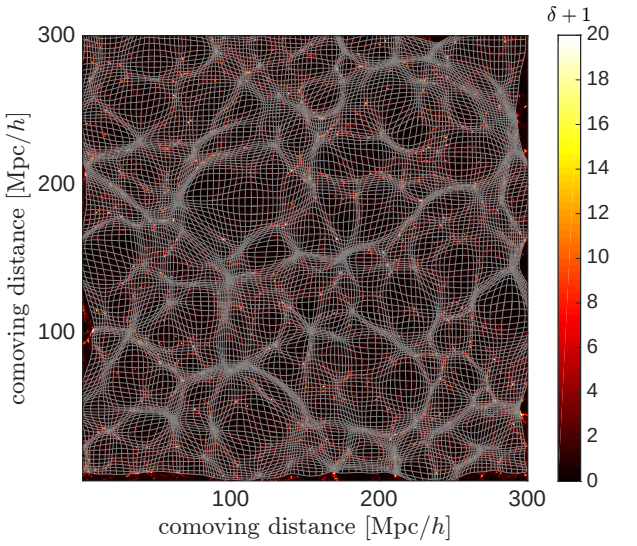

FIG. 1: The 2-D projection of one layer of the deformed grid of a sample N-body simulation is shown as curved white lines. The density fluctuation on the grid, $\delta\rho/\bar{\rho}$, is shown underneath.

The cross power spectrum, $P_{ab}(k)$, is defined as

$$\langle \delta_a(\boldsymbol{k}) \delta_b(\boldsymbol{k'}) \rangle = (2\pi)^3 P_{ab}(k) \delta_{3D}(\boldsymbol{k} - \boldsymbol{k'}), \tag{5}$$

where δ_a and δ_b are any density contrasts and δ_{3D} is the three-dimensional Dirac delta funciton. We typically consider instead the dimensionless power spectrum, $\Delta^2_{ab}(k)$, defined as

$$\Delta^2_{ab}(k) \equiv \frac{k^3 P_{ab}(k)}{2\pi^2}. \tag{6}$$

In the left panel of Fig. 2, we show the matter auto power spectrum ($a = b$) of linear theory density fields (δ_L), from the simulation results (δ_S) and after reconstruction ($\delta_R = -\nabla^2\phi$). For the simulation results, we use the average value of all 130 simulations and show 1σ variances as error bars. To determine the correlation between fields, we compute the cross correlation coefficient $r_{ab}(k) = P_{ab}/\sqrt{P_{aa}P_{bb}}$. In the right panel of Fig. 2, we show r_{SL} and r_{RL}. We see that the reconstructed field is much more highly correlated with the linear field than the simulation field is. For comparison, we also plot the correlation coefficient of δ_E and δ_L as the result in [15], where $\delta_E(\boldsymbol{q}) = -\nabla_q \cdot \boldsymbol{\Psi}(\boldsymbol{q})$ is the negative divergence of the real non-linear displacement from simulaiton. Ideally, MM algorithm aims at getting the cross correlation r_{RL} approaching to r_{EL}. Even though r_{RL} is off the r_{EL} curve in non-linear regime due to the fact that MM reconstruction cannot recover the cell-crossing and vorticity on these scales, we find that on the scale $k \simeq 0.05$ h/Mpc to 0.3 h/Mpc, linear modes were recovered successfully. Specifically, the scale at which $r(k) = 1/2$ drops from $k \simeq 0.2$ h/Mpc to 0.8 h/Mpc after reconstruction. In

comparison with the results of Zhu et al. [12], we find the correlation coefficient falls off at slightly lower wavenumbers, which we attribute to using less particles to run the simulations.

IV. FISHER INFORMATION CONTENT

Mathamatically, the Fisher information I of the initial scale invariant matter power spectrum, A, is defined as

$$I_A \equiv -\left\langle \frac{\partial^2 \ln\mathcal{L}}{\partial A^2} \right\rangle, \tag{7}$$

in which $\mathcal{L}$ denotes the likelihood [16]. In this paper, the word "information" and the symbol "I" both implicitly mean cumulative Fisher information of A. For Gaussian fluctuations, the likelihood depends on parameters only through the power spectrum $P(k)$, so I can be written as

$$I = -\left\langle \sum_{k,k'} \frac{\partial \ln P(k)}{\partial \ln A} \frac{\partial^2 \ln\mathcal{L}}{\partial \ln P(k) \partial \ln P(k')} \frac{\partial \ln P(k')}{\partial \ln A} \right\rangle, \tag{8}$$

in which the angle bracket denotes the average of many realizations of the power spectrum [6].

Eq. 8 can be written in a simpler form in two aspects. First, we can simplify the derivative terms $\partial \ln P(k)/\partial \ln A$. For a given density field δ_a, we can conveniently decompose it into linear and non-linear components

$$\delta_a(k) = b(k)\delta_L(k) + \delta_n(k), \tag{9}$$

in which δ_L denotes the linear density field, $b(k)$ is the bias and $\delta_n(k)$ is defined such that the correlation $\langle \delta_L(k)\delta_n(k)\rangle$ is zero. If we correlate δ_a and δ_L,

$$\langle \delta_a(k)\delta_L(k)\rangle = b(k)\langle \delta_L(k)\delta_L(k)\rangle, \tag{10}$$

we can solve for b as

$$b(k) = \frac{P_{aL}(k)}{P_{LL}(k)}. \tag{11}$$

To find the non-linear term, we correlate δ_a with itself,

$$\langle \delta_a(k)\delta_a(k)\rangle = b^2(k)\langle \delta_L(k)\delta_L(k)\rangle + \langle \delta_n(k)\delta_n(k)\rangle, \tag{12}$$

and find

$$P^2_{aa}(k) = b^2(k)P_{LL}(k) + P_{nn}(k). \tag{13}$$

With the help of Eq. 11 and Eq. 13, we can replace the partial derivatives $\partial \ln P(k)/\partial \ln A$ in Eq. 8 with r^2_{aL}. The second step we can make is to simplify $\partial^2 \ln\mathcal{L}/\partial \ln P(k) \partial \ln P(k')$ by utilizing the fact that its expectation value is the Fisher matrix. For linear fields, this is equal to the inverse of the covariance matrix which is diagonal with elements given by the number of modes in each bin (when considering $\boldsymbol{k}$ and $-\boldsymbol{k}$ as the same mode). We can extend this definition to non-linear fields, provided we take into account that the covariance matrix is no longer diagonal and invert it appropriately [6]. Thus, we can write the Fisher information in terms of matrix multiplication:

$$I\,(< k_n) = r^2(k)^{\mathrm{T}} \left[\mathrm{C}^{-1}_{\mathrm{norm}}(k,k')\right]_{<k_n} r^2(k'), \tag{14}$$

where $\mathrm{C}_{\mathrm{norm}}$ is the normalized covariance matrix defined as

$$\mathrm{C}_{\mathrm{norm}}\,(k,k') = \frac{\mathrm{Cov}(k,k')}{\langle P(k)\rangle\langle P(k')\rangle}, \tag{15}$$

r is the mean cross correlation of a given density field with linear one and the subscript $< k_n$ indicates the matrix is set to zero for modes $k, k' > k_n$. The elements of the covariance matrix are defined as

$$\mathrm{Cov}\,(k,k') \equiv \frac{\sum_{i,j=1}^{N} \left[P_i\,(k) - \langle P\,(k)\rangle\right]\left[P_j\,(k') - \langle P\,(k')\rangle\right]}{N-1}, \tag{16}$$

where N is the total number of simulations and angle brackets are values averaged over all simulations.

The cross-correlation coefficient matrix, or for short the correlation matrix, is defined as :

$$\mathrm{Corr}\,(k,k') = \frac{\mathrm{Cov}\,(k,k')}{\sqrt{\mathrm{Cov}\,(k,k)\,\mathrm{Cov}\,(k',k')}}, \tag{17}$$

and represents the correlation between different k modes. The corelation matrices for non-linear and reconstructed power spectra are shown in the upper-left and lower-right sections of Fig. 3. By definition, the correlation matrix is symmetric with unit diagonal allowing us to overlay the two matrices. For the non-linear case, the correlation matrix is almost diagonal in linear regime, $k \lesssim 0.07\ h/\mathrm{Mpc}$. The off-diagonal elements are produced by strong mode coupling on non-linear scales and the super-survey tidal effect which is small on linear scales but dominates in the weakly non-linear regime [17]. The correlation matrix for the non-linear power spectra has few negative elements ($\mathrm{Corr} \gtrsim -0.18$), which should vanish with more simulations [18]. For the reconstructed correlation matrix, the linear regime expands up to $k \simeq 0.3$ h/Mpc. However, the number and magnitude of negative off-diagonal elements also increases ($\mathrm{Corr} \gtrsim -0.48$).

Cumulative Fisher information is proportional to the volume. We plot the cumulative Fisher information per unit volume of the non-linear, linear and reconstructed power spectra in the left panel of Fig. 4. The Fisher information of the linear power spectra is equal to the number of k modes within the shell in wave space, N_k. We find that the Fisher information of the non-linear power spectra drops from the linear one at $k \simeq 0.05$ h/Mpc, and has a flat plateau in the non-linear regime, with a saturated value of $I \simeq 2.5 \times 10^{-5}/(\mathrm{Mpc/h})^3$. This indicates that there is nearly no independent information in the non-linear regime. However, the information curve of the reconstructed power spectra keeps increasing roughly the same as the linear information until $k \simeq 0.3$ h/Mpc, and reaches a value of $I \simeq 1.3 \times 10^{-3}/(\mathrm{Mpc/h})^3$ at $k \simeq 2.6$ h/Mpc, up by a factor of 50. It means that the MM

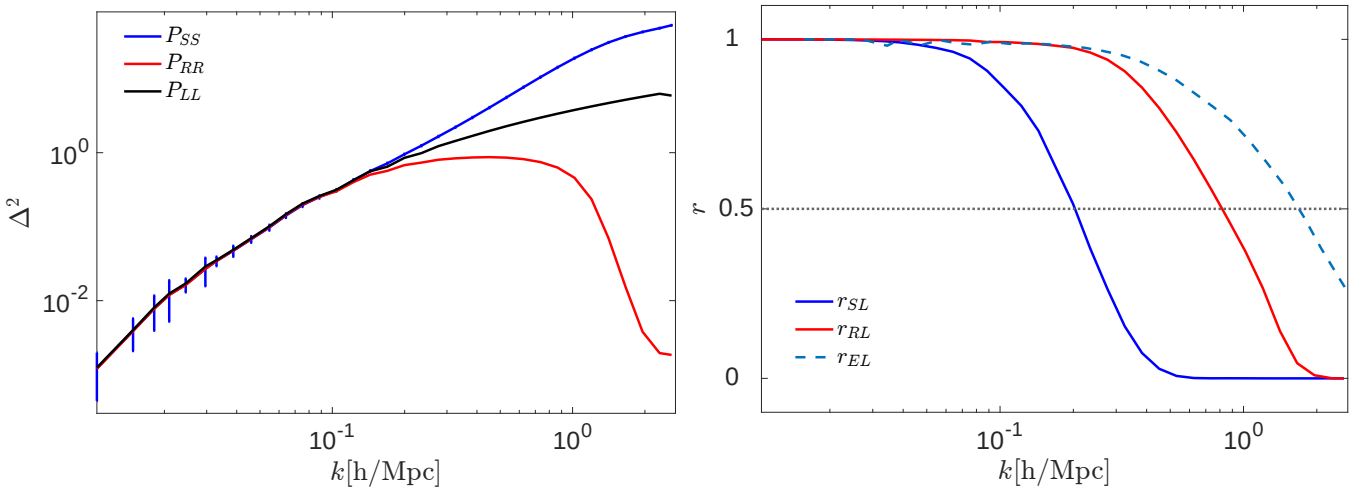

FIG. 2: *Left.* The dimensionless power spectrum computed via linear theory (black), the mean value of 130 N-body simulations with 1σ error bars (blue), and reconstruction of the simulations (red). *Right.* The cross correlation function r_{SL} (blue) and r_{RL} (red), and r_{EL} (dash lines).

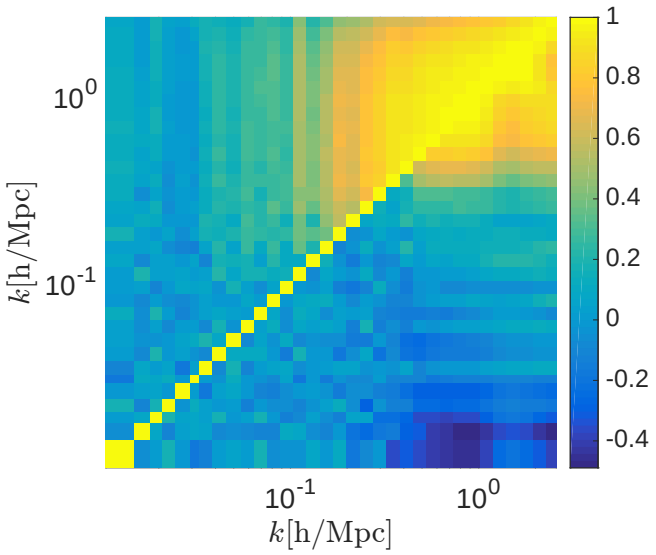

FIG. 3: The correlation matrix as found from 130 non-linear power spectra (the upper-left elements) and the reconstructed power spectra (the lower-right off-diagonal elements).

reconstructed method can strongly recover the lost information within these scales. We compare the Fisher information given by the MM reconstruction method with the logarithmic density mapping method [2] as an example to illustrate its strength. We find that the MM reconstruction gives more than 10 times more information than it.

Another way to efficiently quantify the information is to give the wavenumber κ where the information of linear power spectra has the same magnitude of the given information. In the left panel of Fig. 4, κ is the horizontal coordinates of the intersections of horizonal dotted lines with the linear information curve. At $k \simeq 2.6$ h/Mpc, MM reconstruction push κ from 0.15 h/Mpc to 0.4 h/Mpc, while the logarithmic density mapping method only pushes κ to 0.19 h/Mpc.

In some papers, the cross correlation r^2 terms are set to unity in Eq. 14, which artificially increases the information. For comparison, we plot this case in the right panel of Fig. 4. We see that the logarithmic density mapping information is much higher, but only because it is not well correlated with the initial conditions.

V. CONCLUSION

The MM reconstruction method successfully recovers the lost linear information on mildly non-linear scales and increases the saturated information from $I \simeq 2.5 \times 10^{-5}/((\mathrm{Mpc/h})^3)$ to at least $I \simeq 1.3 \times 10^{-3}/(\mathrm{Mpc/h})^3$. The result is better than previous methods, e.g. [2–4, 19], and we may improve further as the correlation coefficient between the reconstructed and linear fields will increase with higher resolution simulations [12]. This successful result on cold dark matter density fields provides strong motivation to adapt the MM reconstruction scheme to other cosmological fields such as biased tracers like halos and other matter components like baryons and neutrinos.

Acknowledgments

We thank Xin Wang for friendly and helpful discussion, Hong-Ming Zhu for discussion and detailed comments and feedback for the draft and revision, and Yu Yu for discussion and providing the optimized version of the reconstruction code. Computations were performed on the General Purpose Cluster supercomputer at the SciNet HPC Consortium. SciNet is funded by: the Canadian Foundation for Innovation under the auspices of Compute Canada; the Government of Ontario; Ontario Research Fund - Research Excellence; and the University of Toronto.

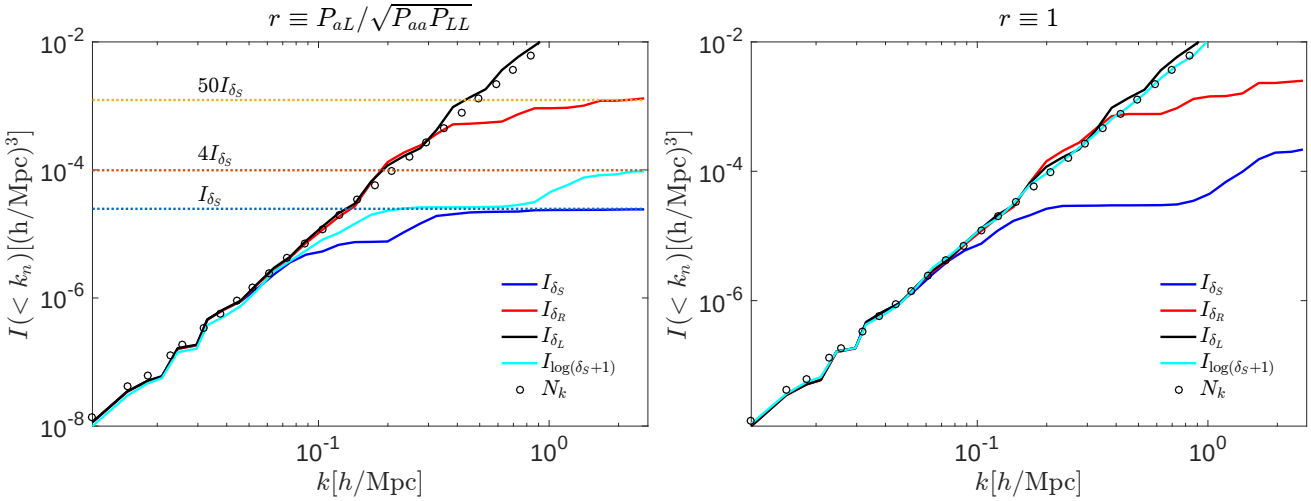

FIG. 4: *Left.* The cumulative Fisher information (solid lines) per unit volume as a function of wavenumber. The blue line corresponds to the non-linear density fields, the red line corresponds to the the reconstructed density fields, the dark line corresponds to the linear density fields, the cyan line corresponds to the logarithmic density mapping, and the circles are number of k modes up to that wave bin. Dotted horizonal lines correspond to value of Fisher information at $k \simeq 2.6$ h/Mpc. *Right.* Same as the left panel except with $r \equiv 1$. The black, blue and cyan lines match the results in [2, 6].

[1] D. H. Weinberg, MNRAS **254**, 315 (1992).
[2] M. C. Neyrinck, I. Szapudi, and A. S. Szalay, ApJ **698**, L90 (2009), 0903.4693.
[3] T.-J. Zhang, H.-R. Yu, J. Harnois-Déraps, I. MacDonald, and U.-L. Pen, ApJ **728**, 35 (2011), 1008.3506.
[4] H.-R. Yu, J. Harnois-Déraps, T.-J. Zhang, and U.-L. Pen, MNRAS **421**, 832 (2012), 1012.0444.
[5] J. Harnois-Déraps, H.-R. Yu, T.-J. Zhang, and U.-L. Pen, MNRAS **436**, 759 (2013), 1205.4989.
[6] C. D. Rimes and A. J. S. Hamilton, MNRAS **360**, L82 (2005), astro-ph/0502081.
[7] D. J. Eisenstein, H.-J. Seo, E. Sirko, and D. N. Spergel, ApJ **664**, 675 (2007), astro-ph/0604362.
[8] Y. B. Zel'dovich, A&A **5**, 84 (1970).
[9] H.-M. Zhu, U.-L. Pen, and X. Chen, ArXiv e-prints (2016), 1609.07041.
[10] U.-L. Pen, ApJS **100**, 269 (1995).
[11] U.-L. Pen, ApJS **115**, 19 (1998), astro-ph/9704258.
[12] H.-M. Zhu, Y. Yu, U.-L. Pen, X. Chen, and H.-R. Yu (2016), 1611.09638.
[13] J. Harnois-Déraps, U.-L. Pen, I. T. Iliev, H. Merz, J. D. Emberson, and V. Desjacques, MNRAS **436**, 540 (2013), 1208.5098.
[14] A. Lewis, A. Challinor, and A. Lasenby, ApJ **538**, 473 (2000), astro-ph/9911177.
[15] H.-R. Yu, U.-L. Pen, and H.-M. Zhu, ArXiv e-prints (2016), 1610.07112.
[16] M. Tegmark, A. N. Taylor, and A. F. Heavens, ApJ **480**, 22 (1997), astro-ph/9603021.
[17] K. Akitsu, M. Takada, and Y. Li, ArXiv e-prints (2016), 1611.04723.
[18] R. Takahashi, N. Yoshida, M. Takada, T. Matsubara, N. Sugiyama, I. Kayo, A. J. Nishizawa, T. Nishimichi, S. Saito, and A. Taruya, ApJ **700**, 479 (2009), 0902.0371.
[19] M. C. Neyrinck, I. Szapudi, and C. D. Rimes, MNRAS **370**, L66 (2006), astro-ph/0604282.